Structure, morphology, and optical properties of $Ga_xIn_{1-x}N_{0.05}As_{0.95}$ quantum wells: Influence of the growth mechanism

W. M. McGee, R. S. Williams, M. J. Ashwin,* and T. S. Jones*,†
Department of Chemistry, Imperial College London, London SW7 2AZ, United Kingdom

E. Clarke and J. Zhang
Department of Physics, Imperial College London, London SW7 2AZ, United Kingdom

S. Tomić
Computational Science and Engineering Department, CCLRC Daresbury Laboratory, Warrington, Cheshire WA4 4AD, United Kingdom
(Received 14 December 2006; published 7 August 2007)

Scanning tunneling microscopy, x-ray diffraction, and photoluminescence spectroscopy have been used to investigate the effects of In concentration and growth temperature on the morphology, structure, and optical properties of GaInNAs quantum wells (QWs) containing 5% N grown by plasma-assisted molecular beam epitaxy. At higher growth temperatures (450 °C) spinodal decomposition and three-dimensional growth readily occurs for high In-content QWs. Lateral segregation of N is enhanced by using higher In concentrations with surface diffusion leading to segregation along an oscillatory strain field that is formed on a planar yet laterally segregated film. Once formed, the N-rich regions alter the band structure and act as quantum-dot-like emitters, with redshifted optical emission. Growth at lower temperatures (400 °C) reduces the extent of spinodal decomposition. The QWs were found to be highly uniform, and the measured emission wavelengths agree very well with values calculated using band anticrossing $\mathbf{k}\cdot\mathbf{p}$ models.

DOI: 10.1103/PhysRevB.76.085309 PACS number(s): 71.20.Nr, 73.21.Fg, 78.66.Fd, 79.60.Bm

I. INTRODUCTION

Understanding how the morphology and structure of GaInNAs quantum wells (QWs) affect their optical properties is of paramount importance if this interesting and relatively new semiconductor alloy is to be successfully employed in optoelectronic device fabrication. GaInNAs is potentially suitable for a variety of devices operating at the two key communications wavelengths of 1.3 and 1.55 μm.[1,2] Considerable progress has been made in the development of 1.3 μm devices,[3,4] but for applications at 1.55 μm, significant challenges remain due to the requirement of high In and N concentration and the low miscibility of N in (In)GaAs.[5,6] Under commonly employed molecular beam epitaxy (MBE) growth conditions, in which N is provided by a plasma source, it is widely reported that increasing the concentration of In and/or N in the QW leads to significant lateral segregation,[6–9] which results in carrier localization and a substantial decrease in emission intensity.[10–13] The segregation effects can be reduced by using a lower growth temperature[14,15] or a higher growth rate,[15] but this can lead to point defects, such as N interstitials, Ga/In vacancies, and As antisites, which also result in poor emission intensity.[17] Postgrowth annealing is commonly used to improve the optical properties of the material. However, any improvements in the structural and optical quality of the as-grown material would clearly be of great benefit for the development of long wavelength devices.

Evidence for spinodal decomposition of GaInNAs into mutually exclusive N-rich and In-rich regions has been provided by cross-sectional transmission electron microscopy (TEM) studies combined with electron energy loss spectroscopy (EELS).[9] The S-shaped temperature dependence of the photoluminescence (PL) emission wavelength has also revealed carrier localization in such samples, another symptom of phase segregation.[10–13] Other evidence for the mutual avoidance of N and In includes reflection high-energy electron diffraction (RHEED) intensity oscillation measurements, which show that the degree of In surface segregation is increased by the inclusion of N.[6] The blueshift of the PL emission wavelength after postgrowth annealing is caused by an increase in the number of In-N bonds in the QW, which, once the sample is grown, reduces the overall strain.[18–23] A large proportion of Ga_4N clusters in as-grown material has been identified using Raman spectroscopy[19] and cross-sectional scanning tunneling microscopy (STM).[20] Two other Raman modes have also been identified, associated with Ga_3InN and segregated GaN,[24] which again serve to illustrate the In and N mutually independent lateral segregation.

At higher growth temperatures, In concentration, and/or N concentration, this phase segregation manifests itself as three-dimensional (3D) growth. We have recently reported a mechanism for the growth mode transition based on spinodal decomposition.[25] On initial deposition, the GaInNAs layer is two-dimensional (2D) but is already laterally decomposed into N-rich (tensile strained) and In-rich (compressively strained) regions, with the neighboring opposing strain fields drastically increasing the overall strain of the film. At some critical thickness, the segregated regions are large enough to relax slightly, which causes a switch to 3D growth as the N-rich regions are not overgrown, leading to the appearance of pits in the films and a rough surface morphology. It is likely that N-rich regions are located at the base of each pit as similar morphologies are observed for GaNAs films grown at high temperatures.[26] The resulting undulating QWs have a poor optical quality, believed to be caused by a high

number of nonradiative centers,[10,17] and in the extreme case dislocations are apparent.[27]

In this paper, we focus on the basic material properties of high N content (5%) GaInNAs QWs grown at different temperatures and with different In contents. A comparison of the measured emission wavelengths with those determined from values calculated from band anticrossing (BAC) $\mathbf{k}\cdot\mathbf{p}$ models reveals a very clear link between the film growth mechanism, the effects of growth temperature and alloy composition, and the resulting properties of the QWs.

II. EXPERIMENTAL DETAILS

All samples were grown in a combined MBE (DCA Instruments)–STM (Omicron Gmbh) system. Epiready GaAs(001) substrates were prepared by thermal desorption of the oxide at 620 °C. A 0.5 μm GaAs buffer layer was then deposited at 590 °C. An As_2 overpressure with an As_2:(In,Ga) flux ratio of ~4:1 was maintained throughout since it has been previously reported that a low V/III ratio can aid the incorporation of substitutional (lattice sites) N.[17,28,29] RHEED intensity oscillations were used to calibrate the incident fluxes of In and Ga. Active N species were provided by an EPI (now Veeco) Unibulb rf plasma source, with the total optical output of the plasma monitored using a silicon photodiode and calibrated to allow selectivity of the incident active N flux. Separate calibration samples were grown and their N content determined by *ex situ* x-ray diffraction (XRD) rocking curves, secondary-ion-mass spectroscopy and PL spectroscopy.

After the deposition of the GaAs buffer layer, the samples were cooled to ~300 °C under an As_2 flux, forming a thin As cap layer to protect the substrate during plasma ignition. Further protection was provided by the N source shutter and the manipulator shutter. The substrate temperature was subsequently lowered to 400–450 °C and a (nominally) 0.5–8 nm thick $Ga_xIn_{1-x}N_yAs_{1-y}$ layer grown at 1.00 ML s^{-1}. The stated layer thicknesses refers to the thickness of a 2D $Ga_xIn_{1-x}N_yAs_{1-y}$ layer assumed to be pseudomorphic. For STM imaging (grown on n^+ GaAs substrates), a 5 nm Ga(N)As spacer layer was inserted prior to $Ga_xIn_{1-x}N_yAs_{1-y}$ deposition to avoid a growth interruption, which would prevent an accurate comparison to the device growth. This Ga(N)As spacer layer is likely to contain ~0.5% N as the plasma-source shutter is not 100% effective. On completion of growth, the samples were quickly removed to the STM chamber with simultaneous closing of all beam shutters, thereby *quenching* the surface and preserving the surface reconstruction and atomic-scale morphology. STM images were then obtained at room temperature in a filled-state mode (4–5 V) and at constant current (0.3–0.5 nA).

Five period multi-QW (MQW) samples were also grown on semi-insulating GaAs for *ex situ* structural (XRD) and optical (PL) analysis. The nominal QW thickness in each sample was 8 nm, the Ga(N)As spacer thickness was 50 nm, and the cap thickness was 200 nm. The N plasma was extinguished immediately following the deposition of the final QW. For PL characterization, samples were placed in a closed-cycle He cryostat. Excitation was provided by a HeNe laser, with the luminescence dispersed by a SPEX 1404 spectrometer and detected with a cooled Ge detector using standard lock-in techniques. High-resolution XRD (004) rocking curves were obtained and analyzed using Philips X'Pert EPITAXY 2.0.

III. RESULTS

The STM images in Fig. 1 show that a range of surface morphologies are adopted when 8 nm thick $Ga_xIn_{1-x}N_{0.05}As_{0.95}$ layers (x=1.0, 0.85, and 0.7) are grown on GaAs(001) substrates at the two different temperatures. The ternary $GaN_{0.05}As_{0.95}$ layer (x=1.0) grown at 400 °C [Fig. 1(a)] has a root-mean-square (rms) roughness of 0.184 nm, whereas the film grown with the same composition at 450 °C [Fig. 1(b)] has a slightly increased rms of 0.201 nm. Neither surface exhibits significant 3D features although they are slightly rougher than GaAs homoepitaxial layers grown under nominally identical conditions. Our previous STM study of relatively high N content GaNAs films revealed an undulating morphology at these growth temperatures. In this current work, the relatively smooth 2D growth is a consequence of the increased growth rate of the layers from 0.5 to 1.0 ML/s, which reduces segregation effects and results in a more planar morphology.[16] Figures 1(c) and 1(d) correspond to 8 nm $Ga_{0.85}In_{0.15}N_{0.05}As_{0.95}$ layers grown at 400 and 450 °C, respectively; a completely uniform alloy of this composition is approximately lattice matched to GaAs. Growth at 400 °C results in a remarkably smooth surface with a rms of 0.177 nm, whereas the film grown at 450 °C has a roughness of 0.341 nm with pits up to 2 nm deep clearly visible in the image. Figures 1(e) and 1(f) show images of 8 nm thick $Ga_{0.7}In_{0.3}N_{0.05}As_{0.95}$ layers; a completely uniform layer of this composition is compressively strained with respect to GaAs. Slight surface roughening can be seen for the film grown at 400 °C, but the overall growth is 2D with a rms of 0.225 nm. For growth at 450 °C, however, the $Ga_{0.7}In_{0.3}N_{0.05}As_{0.95}$ layer is very rough, with pits up to 6 nm deep, an undulation period of ~20 nm, and a rms value of 1.167 nm. Growth under these conditions resulted in a spotty RHEED pattern indicative of pronounced 3D surface features. By contrast, streaked RHEED patterns were observed during the growth of all the other samples.

A deeper understanding of the growth behavior can be obtained by studying the film evolution under conditions that result in surfaces with 3D features. As such, Fig. 2 quantifies the evolution of the STM-determined rms value for each layer as a function of thickness. The observed behavior suggests that the final undulating morphology of the $Ga_{0.7}In_{0.3}N_{0.05}As_{0.95}$ layer grown at 450 °C is a consequence of a Stranski-Krastanow (SK)-type 2D to 3D growth mode transition. Initial deposition of 2 ML, which leads to 2D growth, actually decreases the rms roughness from that of the underlying substrate. This initial flattening is attributed to the presence of In within the growing layer since surface-segregated In is well known to enhance adatom diffusion.[30] Further deposition leads to the onset of 3D growth and a steep increase in the rms values. A less dramatic increase in roughness is measured for the lower In-content

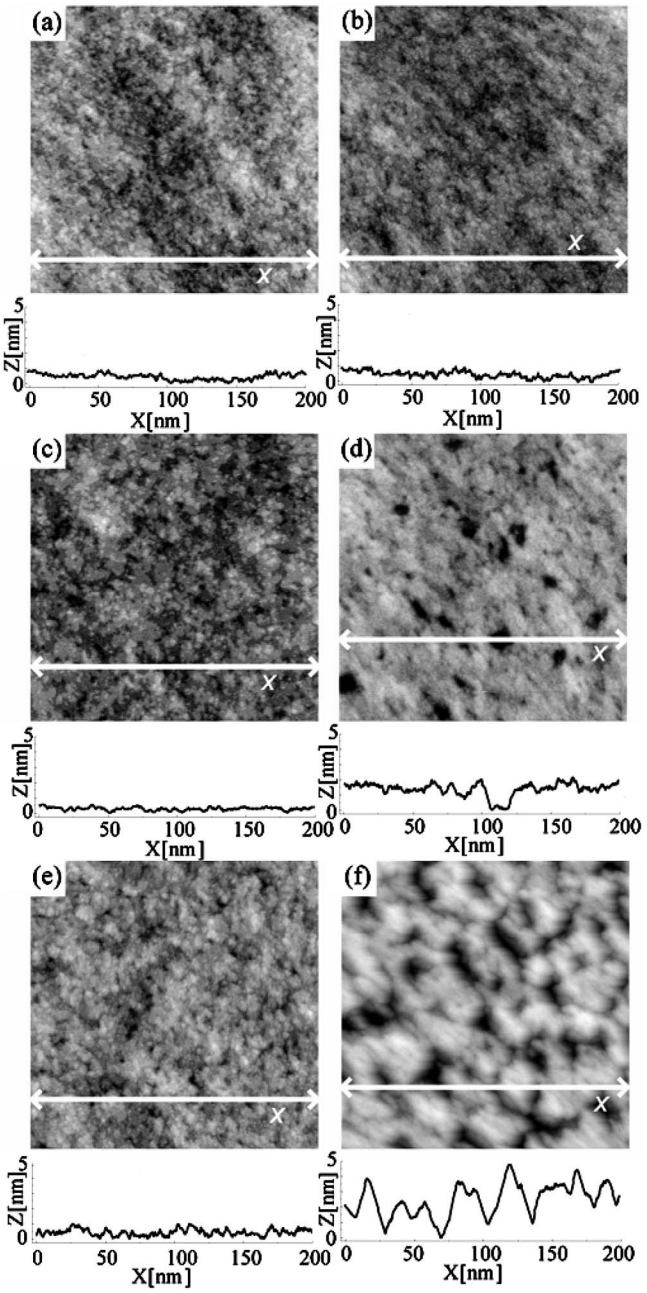

FIG. 1. 200×200 nm^2 filled-state STM images of the surface of single 8 nm thick layers of (a) $GaN_{0.05}As_{0.95}$ grown at 400 °C, (b) $GaN_{0.05}As_{0.95}$ grown at 450 °C, (c) $Ga_{0.85}In_{0.15}N_{0.05}As_{0.95}$ grown at 400 °C, (d) $Ga_{0.85}In_{0.15}N_{0.05}As_{0.95}$ grown at 450 °C, (e) $Ga_{0.7}In_{0.3}N_{0.05}As_{0.95}$ grown at 400 °C, and (f) $Ga_{0.7}In_{0.3}N_{0.05}As_{0.95}$ grown at 450 °C. Beneath each image is the corresponding height cross section marked *X*.

$Ga_{0.85}In_{0.15}N_{0.05}As_{0.95}$ layer grown at 450 °C, with the surface characterized instead by sporadic pits up to 2 nm deep. Lower temperature growth of the $Ga_{0.7}In_{0.3}N_{0.05}As_{0.95}$ layer leads to an approximately constant rms of ~0.22 nm throughout, with no development of significant 3D features. Although the 8 nm thick $Ga_{0.85}In_{0.15}N_{0.05}As_{0.95}$ layer grown at 400 °C is the smoothest of the fully grown layers studied, the initial 2D layer formed during the SK growth of the

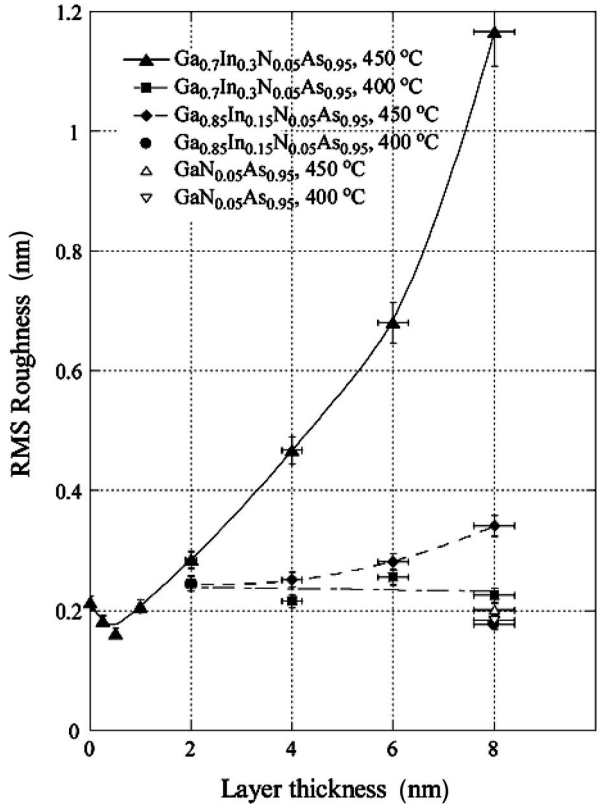

FIG. 2. Evolution of the surface root-mean-square (rms) roughness as a function of film thickness, determined from STM images taken from the surface of single layer $GaN_{0.05}As_{0.95}$, $Ga_{0.85}In_{0.15}N_{0.05}As_{0.95}$, and $Ga_{0.7}In_{0.3}N_{0.05}As_{0.95}$ films. The layers were grown at either 400 or 450 °C.

$Ga_{0.7}In_{0.3}N_{0.05}As_{0.95}$ sample at 450 °C is actually smoother. It is clear from these results that higher In concentrations and/or higher growth temperatures facilitate significant film roughening and a tendency toward 3D growth.

XRD (004) rocking curves for the five period MQW Ga(In)NAs samples ($x=1.0$, 0.85, and 0.7; growth temperatures of 400 and 450 °C) are shown in Fig. 3. All samples were grown using nominally identical plasma conditions. Based on the accuracy of the computer simulation, the error in the XRD-determined alloy composition is ±0.05%. The results show that for all samples, the GaAs spacer layers contain no more than 0.3% N. Figure 3(a) shows the rocking curve for the $GaN_{0.05}As_{0.95}$ MQW sample grown at 400 °C. The simulation reveals that the (nominally) 5% N sample actually contains only 4.2% N in the QWs. An extremely close match to the simulation and the high number of satellite peaks imply high crystalline quality and crisp interfaces between the QWs and the spacer layers. This deviation from Vegard's law has been extensively reported for GaNAs samples,[19,31,32] with the additional N believed to occupy interstitial sites within the lattice. A similar analysis of the $GaN_{0.05}As_{0.95}$ MQW sample grown at 450 °C reveals a much lower measured N concentration of 3.4%. An analysis of the XRD data for the In-containing quaternary MQWs shows that both samples grown at 400 °C contain the full 5% N in each QW. By contrast, higher growth temperatures

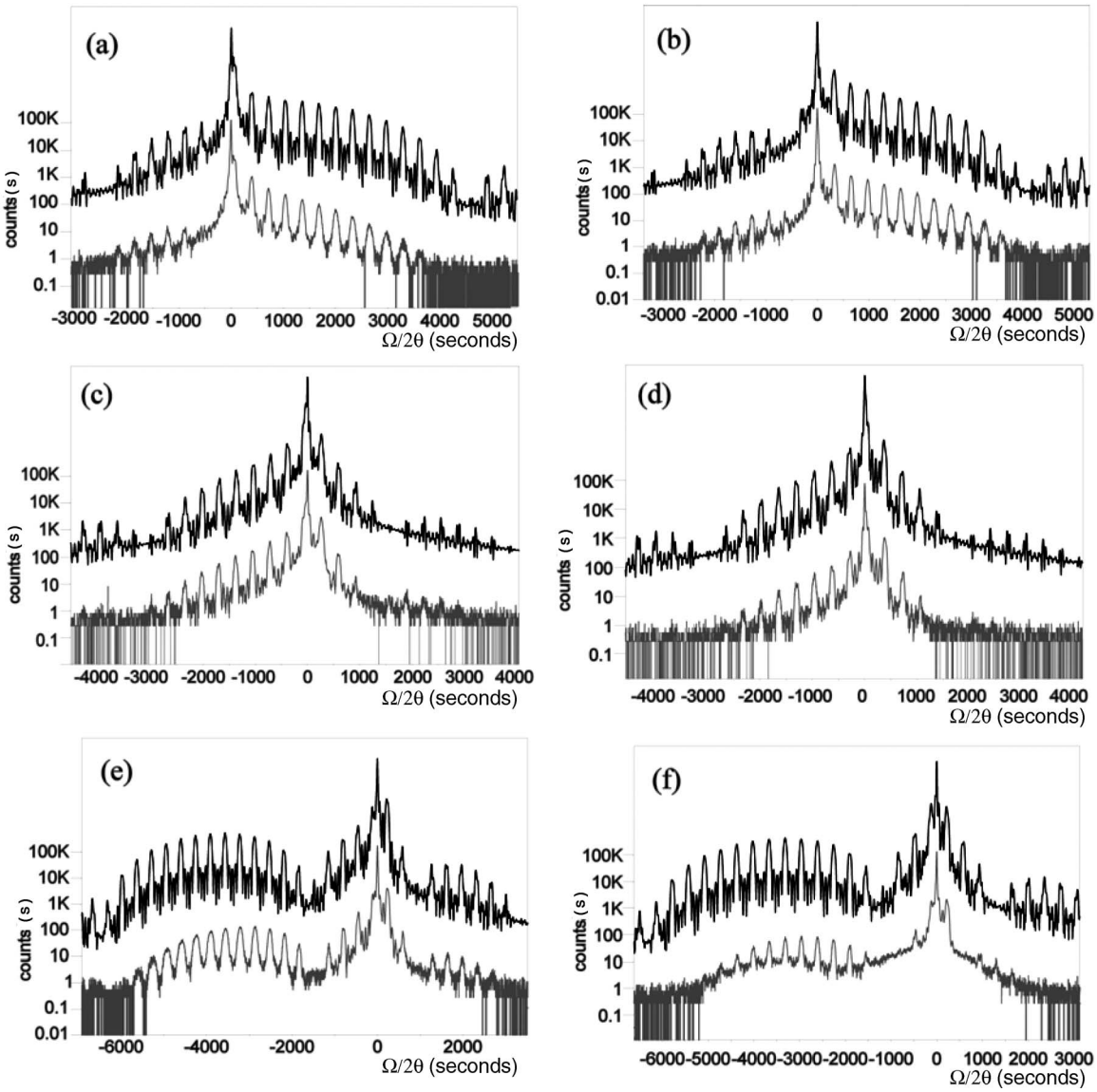

FIG. 3. XRD rocking curves around the (004) reflection for the five period MQW samples containing 8 nm layers of (a) $GaN_{0.05}As_{0.95}$ grown at 400 °C, (b) $GaN_{0.05}As_{0.95}$ grown at 450 °C, (c) $Ga_{0.85}In_{0.15}N_{0.05}As_{0.95}$ grown at 400 °C, (d) $Ga_{0.85}In_{0.15}N_{0.05}As_{0.95}$ grown at 450 °C, (e) $Ga_{0.7}In_{0.3}N_{0.05}As_{0.95}$ grown at 400 °C, and (f) $Ga_{0.7}In_{0.3}N_{0.05}As_{0.95}$ grown at 450 °C. In each, the gray line shows the measured rocking curve, the black line corresponds to the computer simulation.

lead to reduced substitutional N with alloy compositions of 4.2% and 4.0% obtained for $x=0.85$ and 0.7, respectively. For both the ternary and quaternary samples, the higher growth temperature leads to a reduction in the amount of incorporated N occupying lattice sites within the QW.

Low temperature PL data [emission wavelength, intensity, and full width at half maximum (FWHM)] for the six MQW samples are summarized in Table I. Also shown are the emission wavelengths estimated theoretically using the XRD-determined N compositions and structural dimensions. The ground state transition wavelengths were estimated with a 10-band BAC $\mathbf{k}\cdot\mathbf{p}$ Hamiltonian[33] using the tight binding parametrization[34] in the case of GaInNAs. For the GaNAs samples, the 10-band model[35] was expanded into a 12-band BAC $\mathbf{k}\cdot\mathbf{p}$ Hamiltonian to account for N-N cluster states that might lie in close proximity to the conduction band of the GaAs host material.[36–38]

For all layers grown at 400 °C, an extremely close agreement is found between the measured and calculated wavelengths, suggesting that the material is of high compositional uniformity. By contrast, for the samples grown at 450 °C, the measured wavelengths are all significantly redshifted ($\geqslant$90 nm) from the theoretically derived values, the magnitude of the shift increasing with In content (90, 164, and 233 nm for $x=1.0$, 0.85, and 0.7, respectively). For samples of the same nominal composition, the increase in growth temperature produces a significant decrease in emission intensity, with the proportional decrease increasing with In content; the $GaN_{0.05}As_{0.95}$ MQW intensity is reduced by 60%, $Ga_{0.85}In_{0.15}N_{0.05}As_{0.95}$ by 66%, and

TABLE I. Summary of the experimentally determined PL data [emission wavelength, intensity, and full width at half maximum (FWHM)] taken from six GaIn(N)As MQW samples grown with different In compositions (0%, 15% and 30%) and at two different temperatures (400 and 450 °C). The QW widths for each pair of samples are the same. Also listed are the theoretical emission wavelengths calculated using a multiband $\mathbf{k}\cdot\mathbf{p}$ band-anticrossing Hamiltonian and with the QW composition and dimensions determined from experimental XRD measurements. The redshift in the last column refers to the difference between the experimentally and theoretically determined emission wavelength.

Nominal QW structure and growth temperature	Measured N content (%)	Emission wavelength (nm)	Emission intensity (arbs)	Emission FWHM (nm)	Calculated wavelength (nm)	Redshift (nm)
$GaN_{0.05}As_{0.95}$, 400 °C	4.2	1180	6.7	31	1170	10
$GaN_{0.05}As_{0.95}$, 450 °C	3.4	1190	2.7	38	1100	90
$Ga_{0.85}In_{0.15}N_{0.05}As_{0.95}$, 400 °C	5.0	1280	5	49	1302	−28
$Ga_{0.85}In_{0.15}N_{0.05}As_{0.95}$, 450 °C	4.4	1390	1.7	76	1226	164
$Ga_{0.7}In_{0.3}N_{0.05}As_{0.95}$, 400 °C	5.0	1500	30	56	1498	2
$Ga_{0.7}In_{0.3}N_{0.05}As_{0.95}$, 450 °C	4.0	1585	1.5	84	1352	233

$Ga_{0.7}In_{0.3}N_{0.05}As_{0.95}$ by 95%. Broadening of the measured emission is also evident for the increased growth temperature, the extent again increasing with In content.

IV. DISCUSSION

The results presented in Sec. III clearly show that for lower temperature growth, increasing the proportion of In within the alloy causes only marginal variations in rms roughness. It does not affect the XRD-determined N content, and the measured and calculated PL emission wavelengths are in close agreement. By contrast, for higher temperature growth, increasing the In content leads to five major effects: (i) a greater tendency for 3D growth, (ii) a decrease in the XRD-determined N content in the QWs, (iii) an increasing redshift of the emission wavelength, (iv) a significant reduction in emission intensity, and (v) an increased broadening of the emission. In this section, we rationalize this behavior in terms of the growth mechanism.

We have previously proposed a mechanism for morphological breakdown during the growth of a relatively high N-content 2D GaInNAs layer based on spinodal decomposition and the development of a critical oscillatory strain field (OSF) necessitating a switch to 3D growth.[25,26] Addition of In to GaAs causes compressive strain, whereas addition of N leads to tensile strain. The low miscibility of In and N results in spinodal decomposition and lateral phase segregation during the growth of the GaInNAs QW layers.[9] Under certain growth conditions, an initially planar growing layer has a lateral variation in composition due to spinodal decomposition. Compressively strained In-rich regions exist alongside tensile strained N-rich regions. Hence, the overall strain field across the film has an oscillatory behavior. The OSF characteristics depend directly on composition and the degree of segregation in the growing 2D layer. Due to the increased strain between In-rich and N-rich materials, a switch to 3D growth can occur, with an overgrowth of N-rich tensile regions avoided to minimize strain. At lower growth temperatures, surface adatom migration is reduced, which kinetically hinders spinodal decomposition. Consequently, a more uniform metastable alloy is produced.[25]

One-dimensional (1D) representations of the OSFs for each MQW sample grown in this study are shown in Fig. 4. The amplitude of the OSF, defined as $E(x)$, signifies the overall strain between In-rich regions (maxima) and N-rich regions (minima), with $E(x)=0$ corresponding to pure GaAs.

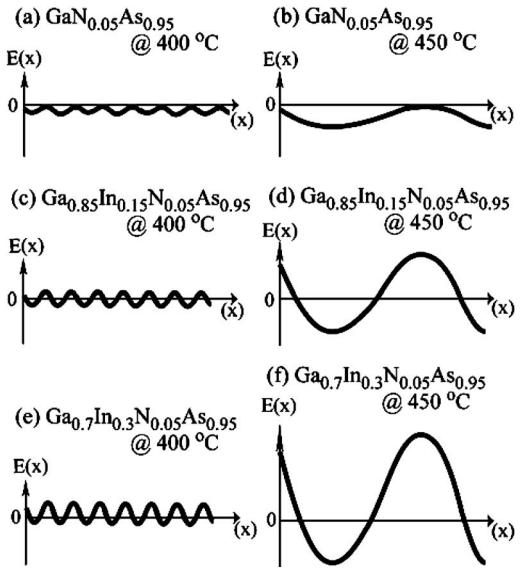

FIG. 4. Schematic representations of the 1D surface oscillatory strain field (OSF), $E(x)$, due to spinodal decomposition during the initial deposition of the dilute nitride alloys when the growth is 2D: (a) $GaN_{0.05}As_{0.95}$ grown at 400 °C, (b) $GaN_{0.05}As_{0.95}$ grown at 450 °C, (c) $Ga_{0.85}In_{0.15}N_{0.05}As_{0.95}$ grown at 400 °C, (d) $Ga_{0.85}In_{0.15}N_{0.05}As_{0.95}$ grown at 450 °C, (e) $Ga_{0.7}In_{0.3}N_{0.05}As_{0.95}$ grown at 400 °C, and (f) $Ga_{0.7}In_{0.3}N_{0.05}As_{0.95}$ grown at 450 °C. A switch from 2D to 3D growth is facilitated if the OSF amplitude is greater than a critical value. The shape of such an OSF determines the initial morphology of the 3D growth, with GaN-rich material based pits forming at minima and InAs-rich mounds forming at maxima.

As a spinodally decomposed 2D layer grows, the amplitude of its OSF will increase until some critical value, at which point a certain degree of lattice relaxation occurs. 3D growth will then occur with pits forming above N-rich material at the OSF minima and In-rich mounds forming at the maxima. Increasing the In content in the alloy makes 3D growth more likely as it increases the amplitude of the OSF. The periodicity of the OSF is determined by the proximity of opposing strain fields and therefore represents the extent of spinodal decomposition. Recent calculations involving the regular solution approximation have suggested that N is the alloy constituent primarily undergoing phase segregation,[8] which is further supported by our reports of 3D GaNAs growth.[26] Studies using TEM-EELS have shown an out-of-phase lateral variation between In-rich and N-rich regions in both flat and undulating QWs. A consideration of the developing OSF can therefore provide a clearer understanding of this apparent repulsion between N and In.

At the higher growth temperature, N-rich clusters form in the growing 2D layer and OSF minima will be generated by the slight relaxation of the tensile N-rich region. On deposition of the next layer, diffusion of group III adatoms will occur from regions of high stress to regions of low stress. Since In atoms are bigger than Ga atoms, an In atom will be more strained when bonded directly above the slightly relaxed N cluster. The resultant effect is that In diffuses away from the relaxed N-rich regions forming In-rich regions and the out-of-phase relationship is established. These compressively strained In-rich regions can then also relax, and an OSF is developed across the growing layer. On further deposition, all in-bound adatoms preferentially diffuse to low stress areas and spinodal decomposition occurs. On average, the N adatoms diffuse to OSF minima, while In adatoms diffuse to the OSF maxima. Lateral In segregation further facilitates lateral N segregation, so the higher the In concentration, the more N segregation there is (and vice versa). The outcome of this feedback effect of enhanced segregation is that both the N-rich and In-rich regions grow and relax further until the OSF reaches critical amplitude and 3D growth follows.

The OSF for the $Ga_{0.7}In_{0.3}N_{0.05}As_{0.95}$ MQW sample grown at 450 °C has an amplitude that is large enough to facilitate a switch to 3D growth, resulting in the undulating morphology seen in the STM image [Fig. 1(f)]. Clearly, a real OSF across a film is unlikely to have the idealized sinusoidal variation shown in Fig. 4, and lateral variations in amplitude will lead to certain regions of the film undergoing 3D growth. This can be seen in the STM image shown in Fig. 1(d), which has a sporadic distribution of 1–2 nm deep pits. The OSF of $GaN_{0.05}As_{0.95}$ grown at 450 °C is still of smaller amplitude, and although it is likely to contain tensile strained N-rich regions, the overall strain is low enough to avoid any measurable pit development [Fig. 1(b)].

Growth at 400 °C kinetically limits the mobility of surface adatoms and hence reduces the tendency for spinodal decomposition. The reduced period and amplitude of the OSFs reflect the localized cancellation of strain fields that occur in the more random alloys. The minima in these samples are more likely to be due to small, randomly occurring N clusters (and even isolated N atoms) in a growing layer, the concentration of which depends statistically on the overall N concentration. These tiny clusters do not relax the lattice sufficiently to increase the OSF amplitude and facilitate further segregation or 3D growth. As surface mobility is limited, these random N clusters are overgrown. Increasing the In content in these lower temperature layers again increases the OSF amplitude although 3D growth is generally avoided due to the lower amplitude OSF. The slight roughening apparent in the $Ga_{0.7}In_{0.3}N_{0.05}As_{0.95}$ layer grown at 400 °C is due to the high In content and higher OSF amplitude.

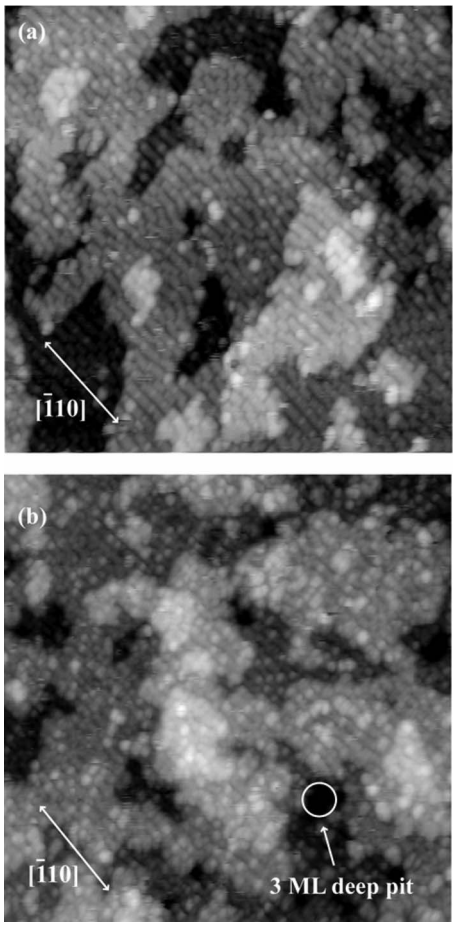

FIG. 5. High-resolution 40×40 nm^2 filled-state STM images taken from the surface of 8 nm thick layers of (a) $Ga_{0.85}In_{0.15}As$ and (b) $Ga_{0.85}In_{0.15}N_{0.05}As_{0.95}$ grown at 400 °C. The $(n\times3)$ surface reconstruction seen in both images is indicative of a structure with a surface-segregated In-rich layer. An example of a small pit up to 3 ML deep is highlighted in the image of the $Ga_{0.85}In_{0.15}N_{0.05}As_{0.95}$ sample.

Although the OSF amplitude increases on the addition of In from $GaN_{0.05}As_{0.95}$ to $Ga_{0.85}In_{0.15}N_{0.05}As_{0.95}$ at 400 °C, the measured rms value actually decreases. Figure 5 compares high-resolution STM images of 8 nm thick $Ga_{0.85}In_{0.15}As$ and $Ga_{0.85}In_{0.15}N_{0.05}As_{0.95}$ layers grown at 400 °C. They both have the same $(n\times3)$ surface reconstruction, which indicates the presence of surface-segregated In. This offers an explanation for the reduction in rms roughness from $GaN_{0.05}As_{0.95}$ to $Ga_{0.85}In_{0.15}N_{0.05}As_{0.95}$ at 400 °C, de-

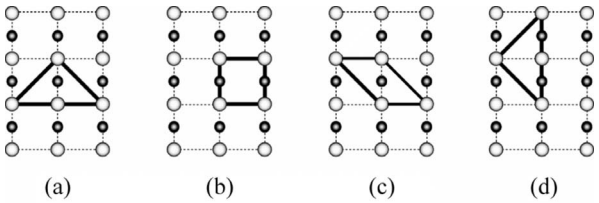

FIG. 6. Schematic illustrating the likelihood of a group III atom being immediately above a cluster of four N atoms in an unreconstructed, randomly distributed, face-centerd-cubic (001) group V layer, containing 5% N. The smaller darker circles represent the uppermost layer, which is group III; the larger paler circles represent the lower layer, which is group V. The solid line in each joins a single permutation of a specific four N atom cluster: (a) has two permutations around the central group III atom, (b) has two, (c) has four, and (d) has two. Based on the number of permutations and the overall N concentration the probability of finding such a group III site is $10(0.05)^4=0.000\,063$. Each four N cluster could relax slightly and increase the strain on a group III atom above, making it migrate away and creating a tiny, transient pit. The more In there is in the layer, the more likely random cluster formation will have an effect of surface roughness, as In would feel the stress of the cluster relaxation to a greater extent and migrate away more readily.

spite the increase in OSF amplitude, as surface-segregated In is well known to aid mobility of surface adatoms and lead to more atomically flat surfaces.[30]

Also seen in the STM image shown in Fig. 5(b) is a tiny ~3 ML deep pit in the 8 nm thick $Ga_{0.85}In_{0.15}N_{0.05}As_{0.95}$ layer grown at 400 °C. Analysis of many regions of the same film shows that a total of 24 of these pits were observed over a surface area of 120 000 nm^2. A possible explanation for their existence is the random formation of tiny N clusters in the alloy. If random N clusters of a certain size form in this growing layer, then subsequent overgrowth is likely to be unfavorable and tiny pits could transiently exist on the growing surface that would be filled in upon further deposition. A calculation of the statistical likelihood of a group III atom being directly above a cluster of four N atoms (see Fig. 6 for different permutations) for an overall N concentration of 5% reveals a probability of 0.0063%. Over a lateral surface area of 120 000 nm^2, this would correspond to, on average, 45 instances of such a bonding arrangement. This group III site would be highly strained (more so for In than for Ga) and thus offers a possible explanation for the observation of the 24 pits in the STM images. Under these growth conditions, the pits are transient and do not deepen and the surface is effectively planar. If we consider the analogous situation for randomly formed N clusters with less than four N atoms, we find a possible explanation for the scale of further roughening observed for the 8 nm thick $Ga_{0.7}In_{0.3}N_{0.05}As_{0.95}$ (at 400 °C) layer: the increased compressive strain due to higher In concentration increasing the OSF amplitude and causing slight roughening. In other words, the observed tiny pits in the $Ga_{0.85}In_{0.15}N_{0.05}As_{0.95}$ layer grown at 400 °C and the slight roughening of the $Ga_{0.7}In_{0.3}N_{0.05}As_{0.95}$ layer grown at 400 °C are likely consequences of random alloy growth.

The XRD results are also consistent with the OSF model. The simulation effectively measures the total strain throughout the layer, which can then be interpreted as the N concentration for a known In content. There are two possible explanations for undermeasurement of the N content: the formation of N-rich clusters and the existence of interstitial N. A spinodally decomposed GaInNAs layer would have both N-rich regions and an enhanced likelihood of interstitial N due to lattice relaxation caused by compositional variation. At higher growth temperatures, there is more surface diffusion and hence more spinodal decomposition, so for nominally identical compositions, an increased growth temperature leads to a reduction in the XRD-determined N content. As previously mentioned, for a spinodally decomposing layer, the feedback effect of In segregation enhances N segregation, and this explains the reduction in the XRD-determined N concentration for increasing In concentration at 450 °C.

The redshift of emission wavelength with increasing growth temperature has previously been attributed to fewer In-N bonds being formed.[10] However, a redshift with increasing growth temperature is also seen for the GaNAs QWs. This suggests that the N-rich regions being formed within the QW layers behave like quantum dots (QDs) with N compositions >5%.

A previously suggested explanation for the observed redshift at higher growth temperatures is provided by *in-situ* annealing during growth of the final capping layer at elevated temperatures.[19,39] It suggests that point defects (such as interstitial N) produced at lower growth temperatures enhance the effectiveness of the *in situ* self-annealing and cause a greater blueshift. This effect may be a contributing factor in postgrowth homogenization of the QWs, but we believe that the extent of the initial spinodal decomposition, reflected in the as-grown STM morphology, is the primary cause of the redshift. Higher growth temperatures favor the formation of GaNAs QD-like regions, with redshifted emission, while subsequent postgrowth annealing serves to homogenize the QWs (whether segregated or randomly alloyed) and produces blueshifted emission for two reasons: (i) more In-N bonds, which reduces the overall strain[18–23] and shifts the minimum of the conduction band edge effectively upward relative to the situation with Ga-N bonds, and (ii) dissolution of the redshifting GaNAs QD-like regions.[7] A larger blueshift has been reported for postgrowth annealing of lower growth temperature MQWs and has been attributed to the redistribution of interstitial N trapped at lower temperatures.[19] Our results suggest that lower growth temperatures lead to a more randomly alloyed QW, which would be better homogenized on postgrowth annealing than a segregated or undulating QW.

The experimentally determined emission wavelengths for the $Ga_{0.85}In_{0.15}N_{0.05}As_{0.95}$ and $Ga_{0.7}In_{0.3}N_{0.05}As_{0.95}$ MQW samples grown at 400 °C show a very good agreement with the wavelengths calculated using the 10-band BAC $\mathbf{k}\cdot\mathbf{p}$ model,[33] using the XRD-determined compositions and structure. A similar good agreement is also obtained for the $GaN_{0.05}As_{0.95}$ MQW sample grown at 400 °C and the 12-band BAC $\mathbf{k}\cdot\mathbf{p}$ model.[36–38] This correlation implies a good, uniform crystal structure and sharp interfaces between the different layers. By contrast, the data shows a significant redshift in emission wavelength for growth at 450 °C for

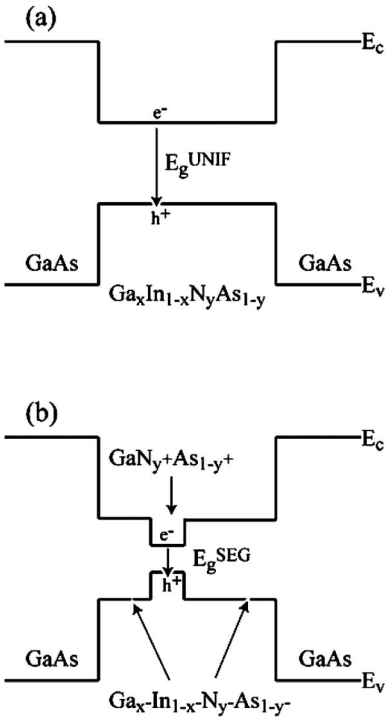

FIG. 7. Schematic of the energy band gap for (a) a uniform GaInNAs QW and (b) a spinodally decomposed GaInNAs QW, with GaN-rich QD-like regions being of lower band gap than the remaining GaIn(N)As material.

samples of the same In and N nominal compositions as in their counterparts grown at lower temperatures. In accordance with the proposed mechanism for higher temperature growth the N-rich (and In-poor) clusters formed by spinodal decomposition are the most likely candidates for these redshifts.

The schematics of the QW band edge structure in Fig. 7 give a qualitative explanation of the redshifted emission coming from GaNAs QD-like structures, with $N>5\%$, embedded within the spinodally decomposed QWs. The BAC model might be questionable for $N>5\%$, so the model cannot be used to calculate the band gap in this case; however, it seems unlikely that the band gap bowing effect does not continue for N concentrations higher than 5%. The amount of redshift for the 450 °C sample increases with In content. A possible explanation for this is the feedback effect of spinodal decomposition: the more In there is, the more N is driven into the segregated N-rich QD-like regions, decreasing their band gap and increasing the emission wavelength.

The proportional decrease in emission intensity on increasing growth temperature reflects the greater 3D character of the layers with higher In content, which is believed to create nonradiative centers.[10,13] The broadening of the spectra with increased growth temperature is also greatest for the higher In-content films, which start to form randomly disordered GaInAs alloys. Furthermore, an increase in line broadening could also be explained by the range of GaNAs QD sizes and N contents that would result, with more In causing more N segregation, which creates a wider variation in the GaNAs QD-like characteristics.

V. SUMMARY

We have investigated the effects of In concentration and growth temperature on the properties of GaInNAs QWs containing a relatively high N concentration of 5%. For a growth temperature of 450 °C, spinodal decomposition readily occurs to create mutual segregation of In and N and a tendency for 3D growth. For higher In concentrations, the extent of N segregation (and therefore 3D growth) is enhanced. Initially, N is the most likely segregating species, which then drives lateral In segregation, giving rise to a feedback effect. The surface diffusion leading to segregation and 3D growth is driven by adatom diffusion from regions of high stress to regions of low stress along an OSF. Once formed, the N-rich regions alter the band structure and act as QD-like emitters, with a red-shifted emission compared to nominally identical layers, grown at lower temperatures.

Growth at lower temperature limits adatom mobility and reduces the extent of spinodal decomposition. All sample grown at 400 °C were highly uniform, and the measured PL emission wavelength is in very close agreement with values calculated using a multiband BAC $\mathbf{k}\cdot\mathbf{p}$ model. Slight roughening is apparent in the STM images of the QWs grown at 400 °C, caused by the random clustering of N in the layer but not by spinodal decomposition.

Our results show a very clear correlation between the alloy growth mechanism and the resulting structural and optical properties of the QWs. They also highlight the importance of gaining a fundamental understanding of the growth behavior of this fascinating but complex material system.

ACKNOWLEDGMENTS

The authors acknowledge the financial support of the Engineering and Physical Sciences Research Council (EPSRC), UK via the Ultra-Fast Photonics Collaboration (UPC). Computing resources were provided by CCLRC's e-Science facility.

*Present address: Department of Chemistry, University of Warwick, Coventry, CV4 7AL, UK.
†t.s.jones@warwick.ac.uk

[1] M. Kondow, K. Uomi, A. Niwa, T. Kitatani, S. Wakahiki, and Y. Yazawa, Jpn. J. Appl. Phys., Part 1 **35**, 1273 (1996).
[2] A. J. Ptak, D. J. Friedman, S. Kurtz, and J. Kiehl, 31st IEEE Photovoltaic Specialists Conference and Exhibition, Florida (unpublished), p. 707.
[3] N. Tansu and L. J. Mawst, IEEE Photonics Technol. Lett. **14**, 444 (2002).
[4] R. Fehse, S. Tomić, A. R. Adams, S. J. Sweeney, E. P. O'Reilly, A. Andreev, and H. Riechert, IEEE J. Sel. Top. Quantum Electron. **8**, 801 (2002).
[5] J. Neugebauer and C. G. Van de Walle, Phys. Rev. B **51**, 10568

(1995).
[6] H. F. Liu, N. Xiang, and S. J. Chua, Appl. Phys. Lett. **89**, 071905 (2006).
[7] L. Grenouillet, C. Bru-Chevallier, C. Guillot, P. Gilet, P. Ballet, P. Duvaut, G. Rolland, and A. Million, J. Appl. Phys. **91**, 5902 (2002).
[8] M. Herrera, D. González, M. Hopkinson, M. Gutiérrez, P. Navaretti, H. Y. Liu, and R. Garcia, J. Appl. Phys. **97**, 073705 (2005).
[9] X. Kong, A. Trampert, and K. H. Ploog, Micron **37**, 465 (2006).
[10] L. Geelhaar, M. Galluppi, G. Jaschke, R. Averbeck, H. Riechert, T. Remmele, M. Albrecht, M. Dworzak, R. Hildebrant, and A. Hoffmann, Appl. Phys. Lett. **88**, 011903 (2006).
[11] H. D. Sun, A. H. Clark, S. Calvez, M. D. Dawson, P. Gilet, L. Grenouillet, and A. Million, J. Appl. Phys. **97**, 033517 (2005).
[12] A. Patanè, J. Endicott, J. Ibánez, P. N. Brunkov, L. Eaves, S. B. Healy, A. Lindsay, E. P. O'Reilly, and M. Hopkinson, Phys. Rev. B **71**, 195307 (2005).
[13] A. Hierro, J.-M. Ulloa, J.-M. Chauveau, A. Trampert, M.-A. Pinault, E. Tournié, A. Guzmán, J. L. Sánchez-Rojas, and E. Calleja, J. Appl. Phys. **94**, 2319 (2003).
[14] K. Volz, T. Torunski, and W. Stolz, J. Appl. Phys. **97**, 014306 (2005).
[15] D. Litvinov, D. Gerthsen, A. Rosenauer, M. Hetterich, A. Grau, P. Gilet, and L. Grenouillet, IEE Proc.: Optoelectron. **151**, 275 (2004).
[16] J. F. Chen, R. S. Hsiao, P. C. Hsieh, J. S. Wang, and J. Y. Chi, J. Appl. Phys. **99**, 123718 (2006).
[17] H. Y. Liu, C. M. Tey, C. Y. Jin, S. L. Liew, P. Navaretti, M. Hopkinson, and A. G. Cullis, Appl. Phys. Lett. **88**, 191907 (2006).
[18] S. G. Spruyette, C. W. Coldren, J. S. Harris, W. Wampler, P. Krispin, K. Ploog, and M. C. Larson, J. Appl. Phys. **89**, 4401 (2001).
[19] E.-M. Pavelescu, J. Wagner, H.-P. Komsa, T. T. Rantala, M. Dumitrescu, and M. Pessa, J. Appl. Phys. **98**, 083524 (2005).
[20] R. Duca, G. Ceballos, C. Nacci, D. Furlanetto, P. Finetti, S. Modesti, A. Cristofoli, G. Bais, M. Piccin, S. Rubini, F. Martelli, and A. Franciosi, Phys. Rev. B **72**, 075311 (2005).
[21] V. Lordi, H. B. Yuen, S. R. Bank, M. A. Wistey, J. S. Harris, and S. Friedrich, Phys. Rev. B **71**, 125309 (2005).
[22] G. Mussler, L. Däweritz, and K. H. Ploog, Appl. Phys. Lett. **87**, 081903 (2005).
[23] K. Uno, M. Yamada, I. Tanaka, O. Ohtsuki, and T. Takizawa, J. Cryst. Growth **278**, 214 (2005).
[24] T. Tite, O. Pagès, and E. Tournié, Appl. Phys. Lett. **85**, 5872 (2004).
[25] W. M. McGee, R. S. Williams, M. J. Ashwin, and T. S. Jones, Surf. Sci. **600**, L194 (2006).
[26] W. M. McGee, P. A. Bone, R. S. Williams, M. J. Ashwin, and T. S. Jones, Appl. Phys. Lett. **87**, 181905 (2005).
[27] M. Herrera, D. González, R. García, M. Hopkinson, P. Navaretti, M. Gutiérrez, and H. Y. Liu, Thin Solid Films **483**, 185 (2005).
[28] F. Ishikawa, M. Höricke, U. Jahn, A. Trampert, and K. H. Ploog, Appl. Phys. Lett. **88**, 191115 (2006).
[29] T. Hakkarainen, E.-M. Pavelescu, and J. Likonen, Physica E (Amsterdam) **32**, 266 (2006).
[30] W. M. McGee, T. J. Krzyzewski, and T. S. Jones, J. Appl. Phys. **99**, 043505 (2005).
[31] M. Reason, H. A. McKay, W. Ye, S. Hanson, R. S. Goldman, and V. Rotberg, Appl. Phys. Lett. **85**, 1692 (2004).
[32] W. J. Fan, S. F. Yoon, T. K. Ng, S. Z. Wang, W. K. Loke, R. Liu, and A. Wee, Appl. Phys. Lett. **80**, 4136 (2002).
[33] S. Tomić, E. P. O'Reilly, R. Fehse, S. J. Sweeney, A. R. Adams, A. D. Andreev, S. A. Choulis, T. J. C. Hosea, and H. Riechert, IEEE J. Sel. Top. Quantum Electron. **9**, 1228 (2003).
[34] A. Lindsay and E. P. O'Reilly, Physica B **340-342**, 434 (2003).
[35] S. Tomić, E. P. O'Reilly, P. J. Klar, H. Grüning, W. Heimbrodt, W. M. Chen, and I. A. Buyanova, Phys. Rev. B **69**, 245305 (2004).
[36] S. Fahy and E. P. O'Reilly, Physica E (Amsterdam) **91**, 881 (2004).
[37] S. B. Healy, A. Lindsay, and E. P. O'Reilly, IEE Proc.: Optoelectron. **151**, 397 (2004).
[38] E. P. O'Reilly, (private communication).
[39] E.-M. Pavelescu, T. Jouhti, M. Dumitrescu, P. J. Klar, S. Karirinne, Y. Fedorenko, and M. Pessa, Appl. Phys. Lett. **83**, 1497 (2003).